ARTICLE

Ab initio Predictions of Structural and Thermodynamic Properties of Zr_2AlC Under High Pressure and High Temperature

Fen Luo[a*], Zhi-cheng Guo[a], Xiu-lu Zhang[a], Chang-ying Yuan[a], Ling-cang Cai[b]

a. Laboratory for Extreme Conditions Matter Properties, Southwest University of Science and Technology, Mianyang 621900, China
b. National Key Laboratory for Shock Wave and Detonation Physics Research, Institute of Fluid Physics, Chinese Academy of Engineering Physics, Mianyang 621900, China

(Dated: Received on March 8, 2015; Accepted on April 23, 2015)

The structural and thermodynamic properties of Zr_2AlC at high pressure and high temperature are investigated by first principles density functional theory method. The calculated lattice parameters of Zr_2AlC are in good agreement with the available theoretical data. The pressure dependences of the elastic constants, bulk modulus, shear modulus, Young's modulus, and Vickers hardness of Zr_2AlC are successfully obtained. The elastic anisotropy is examined through the computation of the direction dependence of Young's modulus. By using the quasiharmonic Debye model, the thermodynamic properties including the Debye temperature, heat capacity, volume thermal expansion coefficient, and Grüneisen parameter at high pressure and temperature are predicted for the first time.

Key words: Elastic property, Thermodynamic property, Density functional theory

I. INTRODUCTION

$M_{n+1}AX_n$ (MAX) phases, where M is an early transition metal, A is a group IIIA or IVA element, and X is either C or N, have been attracting extensive interests due to their unusual properties combining the merits of both ceramics and metals [1−3]. The MAX phases have many advantage such as high thermal and electrical conductivity, fully reversible plasticity, good damage tolerance, exceptional shock resistance, quite stiffness and relatively lightness and so on [1−5]. MAX phases crystallize in the space group of $P6_3/mmc$ [6], where blocks of transition metal carbide or nitride formed by edge-shared M_6X octahedra are sandwiched with A atomic sheets. In 1970s, Nowotny's group synthesized more than 100 new MAX phases for the first time [7]. Palmquist *et al*. made a breakthrough on a new phase Ti_4SiC_3, which was deposited on MgO (111) and Al_2O_3 (0001) using magnetron sputtering method [8]. Later, more new MAX phases have been reported, including V_4AlC_3 [9] and Nb_4AlC_3 [10].

In order to fully take advantage of the properties of MAX phases for eventual technological applications, a number of experiments and theoretical calculation have been carried out [11−16]. Through the room temperature synchrotron X-ray diffraction experiments, Kumar *et al*. reported that the layered hexagonal ternary carbide Nb_2AsC was stable with no phase transitions observed in a diamond anvil cell to a pressure of 41 GPa [11]. Music *et al*. investigated the phase stability and elastic properties of $Ta_{n+1}AlC_n$ (n=1−3) at high pressure and high temperature using *ab initio* calculations [12]. Brika *et al*. presented the hydrostatic pressure effects on the structural and elastic properties of Nb_2InC ternary carbide based on first principles calculations [13]. Recently, using first-principles plane-wave pseudopotential density functional theory (DFT), the structural parameters, elastic and electronic properties of Nb_2AC (A=S and In) phases were investigated by Romeo *et al*. [14]. However, up to now, only Yakoubi *et al*. [15] and Bouhemadou *et al*. [16] performed the theoretical investigations on the electronic and elastic properties of layered ternary carbide Zr_2AlC and the investigations on the structural and thermodynamic properties of the Zr_2AlC at high pressure and high temperature are still lacking. Therefore, in the present work, we describe a systematical investigation of the structural and thermodynamic properties of the layered ternary carbide Zr_2AlC at high pressure and high temperature.

II. COMPUTATIONAL METHOD

The total energy calculations are performed on the basis of the DFT, as implemented in the cambridge serial total energy package program [17]. After testing, the generalized gradient approximation [18] and ultrasoft pseudopotential are employed. For integration within the Brillouin zone, specific k points are selected using a 9×9×2 Monkhorst-Pack grid for Zr_2AlC.

*Author to whom correspondence should be addressed. E-mail: luofen11@126.com

TABLE I Calculated lattice constants a and c, internal free coordinate z, bulk modulus B and its pressure derivative B', along with the other theoretical results.

	a/Å	c/Å	c/a	z	B/GPa	B'/GPa
This work	3.3174	14.6304	4.4102	0.0861	124.04	4.0836
Calculated. [15]	3.2104	14.2460	4.437	0.08693	176.28	4.01
Calculated. [16]	3.26899	14.40815	4.40753	0.08646	134	3.89

The plane-wave cutoff energy is selected to be 400 eV. The set of parameters for geometry optimization ensures the convergence of energy of 1.0×10^{-5} eV/atom, the maximum force of 0.03 eV/Å, the maximum stress of 0.05 GPa and the maximum ionic displacement of 0.001 Å.

III. RESULTS AND DISCUSSION

A. Structural properties

At ambient pressure, Zr_2AlC crystallizes in the hexagonal structure with the $P6_3/mmc$ space group, and whose atoms occupy the Wyckoff positions as follows: 2a (0, 0, 0) for C, 2d (1/3, 2/3, 3/4) for Al and 4f (1/3, 2/3, z) for Zr, where z is the internal free coordinate. The Zr_2AlC structure is optimized at fixed pressure in the range from 0 GPa to 40 GPa with the step of 2 GPa. The relaxed cell parameters, together with other theoretical results [15, 16] are listed in Table I. It can be seen that the calculated lattice constant a and c, internal free coordinate z agree well with the theoretical data [15, 16]. The good agreement between them shows the accuracy of the present structural calculations.

The obtained Birch-Murnaghan equation of state (EOS) [19] is used to calculate cell volumes at different pressures and fitted as follows:

$$P=\frac{3}{2}B(x^{-7/3}-x^{-5/3})\left[1+\frac{3}{4}(B'-4)(x^{-2/3}-1)\right] \quad (1)$$

where x stands for V/V_0 and P stands for pressure. B is the bulk modulus and B' is its pressure derivative. The results of B and B' are also shown in Table I. The calculated bulk modulus values are in agreement with the first principles calculations of Yakoubi *et al.* [15] and Bouhemadou1 *et al.* [16]. In Fig.1, we present the pressure dependences of calculated normalized lattice parameters a/a_0, c/c_0, and V/V_0 of Zr_2AlC (where a_0, c_0, and V_0 are the zero pressure equilibrium structure parameters) at zero temperature. We clearly observe a quadratic dependence in all curves of Zr_2AlC in the applied pressure. It is shown that the equilibrium ratio c/c_0 decreases more quickly than a/a_0 with the pressure increasing, indicating that the compression along c axis is larger. For the internal free coordinate z, it increases with the pressure increasing. By fitting the z-P data to a second-order polynomial, we have the following relations:

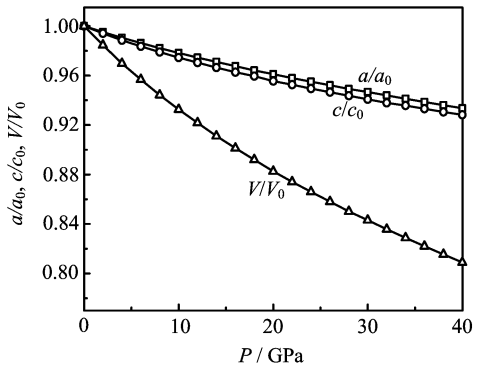

FIG. 1 The normalized lattice parameters (a/a_0 and c/c_0) and volume V/V_0 as a function of pressure from 0 GPa to 40 GPa for Zr_2AlC at 0 K.

$$z = 0.0862 + 2.2159\times10^{-4}P - 1.6034\times10^{-6}P^2 \quad (2)$$

It can be found that the internal free coordinate z increases from 0.0861 at 0 GPa to 0.0926 at 40 GPa, with an increase of about 7.54%.

B. Mechanical stability and elastic properties

Elastic properties of a solid are important because they are closely related to various fundamental solid-state phenomena, such as EOS, phonon spectra, and atomic potentials. Most importantly, knowledge of elastic constants is essential for many practical applications related to the mechanical properties of a solid, such as internal strain, thermoelastic stress, and load deflection. In order to further confirm the structure stability under strain, the elastic constants of Zr_2AlC are calculated, which are shown in Table II. For a hexagonal structure, there are six independent elastic constants C_{11}, C_{12}, C_{13}, C_{33}, C_{44}, and C_{66}. The mechanical stability criteria are given by $\widetilde{C}_{44}>0$, $\widetilde{C}_{11}>|\widetilde{C}_{12}|$, $\widetilde{C}_{33}(\widetilde{C}_{11}+\widetilde{C}_{12})>2\widetilde{C}_{13}^2$ [20] with:

$$\begin{aligned}\widetilde{C}_{\alpha\alpha} &= C_{\alpha\alpha} - P \quad (\alpha = 1,3,4)\\ \widetilde{C}_{12} &= C_{12} + P\\ \widetilde{C}_{13} &= C_{13} + P\end{aligned} \quad (3)$$

The calculated elastic constants satisfy all these criteria, which implies that Zr_2AlC is mechanically stable in the applied pressure.

DOI:10.1063/1674-0068/28/cjcp1503032

TABLE II Calculated elastic constants C_{ij} (GPa) of Zr_2AlC compared with the theoretical data.

	C_{11}	C_{12}	C_{13}	C_{33}	C_{44}	C_{66}
This work	266.08	55.91	63.07	226.77	87.75	105.08
Calc. [16]	284	64	67	235	97	107

The elastic constants C_{ij} of Zr_2AlC as a function of the hydrostatic pressure are shown in Fig.2(a). Noticeably, there exhibits a quasi-linear dependence between the elastic constants and hydrostatic pressure for Zr_2AlC as the applied pressure ranges from 0 GPa to 20 GPa. By comparing these elastic constants, C_{33} is the most sensitive constant to the hydrostatic pressure, whereas C_{66} is the least sensitive one. From the obtained elastic constants, the Voigt B_V, G_V, Reuss B_R, and G_R can be expressed as [21]:

$$B_V = \frac{1}{9}(2C_{11} + C_{33} + 2C_{12} + 4C_{13}) \quad (4)$$

$$B_R = \frac{(C_{11} + C_{12})C_{33} - 2C_{13}^2}{C_{11} + C_{12} + 2C_{33} - 4C_{13}} \quad (5)$$

$$G_V = \frac{1}{30}[M + 12C_{44} + 12C_{66}] \quad (6)$$

$$G_R = \frac{5}{2}\frac{C^2 C_{44} C_{66}}{3B_V C_{44} C_{66} + C^2(C_{44} + C_{66})} \quad (7)$$

$$M = C_{11} + C_{12} + 2C_{33} - 4C_{13} \quad (8)$$

$$C^2 = (C_{11} + C_{12})C_{33} - 2C_{13}^2 \quad (9)$$

Hill [22] shows that the polycrystalline modulus are the arithmetic mean values of the Voigt and Reuss modulus and thus given by:

$$B = \frac{B_V + B_R}{2} \quad (10)$$

$$G = \frac{G_V + G_R}{2} \quad (11)$$

Then, Young's modulus E can be calculated by:

$$E = \frac{9BG}{3B + G} \quad (12)$$

As listed in Table III, the bulk modulus B deduced from elastic constants turns out to be very close to that obtained by Birch-Murnaghan EOS fitting. This indicates that our calculations are consistent and reliable. The B, G, E increase monotonously with the pressure increasing, as presented in Fig.2(b).

To investigate the hardness of crystal, the microscopic hardness model proposed by Chen *et al.* [23] can be adopted. Based on this model, the hardness of crystal can be expressed as follows:

$$H_V = 2(k^2 G)^{0.585} - 3 \quad (13)$$

TABLE III Polycrystalline elastic properties of Zr_2AlC, including B, G, E, k, Vickers hardness H_V, and Debye temperature Θ.

P/GPa	B/GPa	G/GPa	E/GPa	k	H_V/GPa	Θ/K
0	124.56	94.16	225.64	0.76	17.59	482.32
2	132.60	96.39	232.77	0.73	16.93	487.22
4	139.31	98.76	239.66	0.71	16.64	492.26
6	148.06	101.15	247.16	0.68	16.07	497.51
8	155.34	103.15	253.37	0.66	15.66	501.67
10	162.32	106.89	262.94	0.66	15.86	509.71
12	170.28	109.33	270.16	0.64	15.56	514.83
14	178.02	111.74	277.22	0.63	15.31	519.77
16	185.93	113.41	282.74	0.61	14.86	523.06
18	193.94	115.20	288.48	0.59	14.47	526.59
20	199.05	118.41	296.44	0.59	14.78	532.92

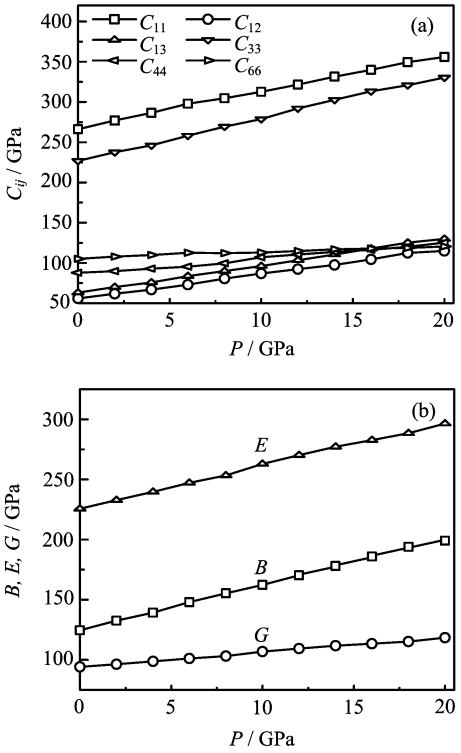

FIG. 2 (a) Elastic constants C_{ij} as a function of pressure P at zero temperature. (b) Bulk modulus B, shear modulus G, and Young's modulus E as a function of pressure P at zero temperature.

where k=G/B is Pugh's modulus ration. Pugh has proposed an empirical criterion by the ratio of k to distinguish them: if k>0.57, a material behaves in a brittle manner, otherwise it behaves in a ductile manner [24]. At 0 GPa, the ratio of k is 0.76, which indicates the brittle manner of Zr_2AlC. Table III shows the effect of pressure on the ratio k. It shows that the values of k are larger than 0.57 as the applied pressure ranges from 0 GPa to 20 GPa, demonstrating that Zr_2AlC

DOI:10.1063/1674-0068/28/cjcp1503032

is still brittle with increasing pressure. Based on the above discussed hardness model, the Vickers hardness of Zr_2AlC is presented in Table III. It shows that the theoretical Vickers hardness of Zr_2AlC is 17.59 GPa at 0 GPa, and the Vickers hardness of Zr_2AlC decreases with increasing pressure.

The velocities of longitudinal and transverse wave V_l and V_t, and the average acoustic velocity V_m can be calculated by [25]:

$$V_l = \left[\frac{B + 4/3G}{\rho}\right]^{1/2} \tag{14}$$

$$V_t = \left(\frac{G}{\rho}\right)^{1/2} \tag{15}$$

$$V_m = \left[\frac{2/V_t^3 + 1/V_l^3}{3}\right]^{-1/3} \tag{16}$$

Finally, the Debye temperature Θ can be derived via [25]:

$$\Theta = \frac{h}{k_B}\left[\frac{3n}{4\pi}\left(\frac{N}{V}\right)\right]^{1/3} V_m \tag{17}$$

where h is the Plank constant, k_B is the Boltzmann constant, n is the number of atoms in the formula unit, N is the number of formula in the cell volume V. The results are presented in Table III. It can be seen that the Debye temperatures increase with increasing pressure.

To further evaluate the elastic anisotropy of Zr_2AlC, we give the direction-dependent E. And the expression can be expressed as [26]:

$$E = \frac{1}{(1-l_3^2)^2 S_{11} + l_3^4 S_{33} + l_3^2(1-l_3^2)(2S_{13}+S_{44})} \tag{18}$$

where l_1, l_2, and l_3 represent the direction cosines with respect to the x, y, and z axis, respectively. Using the calculated compliance constant S_{ij}, the direction dependence of the Young's modulus of Zr_2AlC is obtained and shown in Fig.3. The projected directional E in the x-y plane is greatly different from that of the x-z and y-z planes, which reveals the elastic anisotropy of Zr_2AlC.

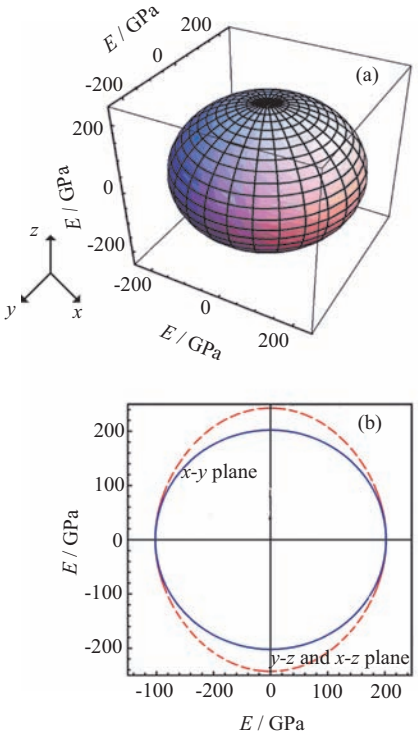

FIG. 3 Direction dependence of Young's modulus (a) and its projections onto the x-y, y-z, and x-z planes (b) for Zr_2AlC.

C. Thermodynamic properties

The investigations on the thermodynamic properties of materials at high pressure and high temperature are an interesting topic in the condensed matter physics. To gain deeper insights into the thermodynamic properties of the layered ternary carbide Zr_2AlC, we apply the quasiharmonic Debye model [27]. The Θ is one of the important thermodynamic parameters, and is used to distinguish between high- and low-temperature regimes. If $T>\Theta$, one expects all phonon modes to have energy k_BT, and if $T<\Theta$, we expect high-frequency modes to be frozen [25]. The variation of the Θ of Zr_2AlC as a function of temperature at different pressures are illustrated in Fig.4(a). It can be seen that at low pressure, the Θ decreases with increasing temperature. The temperature effects are suppressed by pressure, especially under high pressure. Figure 4(b) shows the heat capacity C_V of Zr_2AlC for various pressures. It can be seen that the heat capacity C_V increases exponentially with the temperature at $T<600$ K. At higher temperature $T>600$ K, the heat capacity C_V is very close to a constant.

Figure 5 shows the variation of Θ and C_V with pressure and temperature. They are normalized by $(X-X_0)/X_0$, where X and X_0 are the Θ or C_V at any pressure and zero pressure at 300 and 2000 K. It can be seen that at a given temperature, the Θ increases almost linearly with increasing pressure. The Θ at 2000 K are higher than those at 300 K, which shows the fact that the vibration frequency of the particles in Zr_2AlC changes with the pressure and temperature. When the temperature keeps constant, the C_V decreases with the applied pressures increasing.

The volume thermal expansion coefficient α as functions of pressure and temperature are plotted in Fig.6. From Fig.6(a) we can see that the volume thermal expansion coefficient α is proportional T^3 at low temperature and gradually approaches to a linear increase at high temperature. The volume thermal expansion coefficient decreases strongly with increasing pressure in Fig.6(b). The value of Grüneisen parameter γ versus

DOI:10.1063/1674-0068/28/cjcp1503032

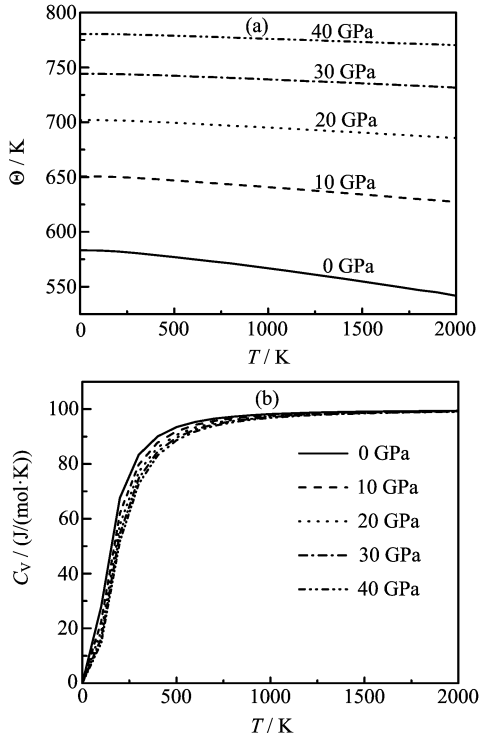

FIG. 4 Variation of (a) the Θ and (b) C_V with the temperature at different pressures for Zr_2AlC.

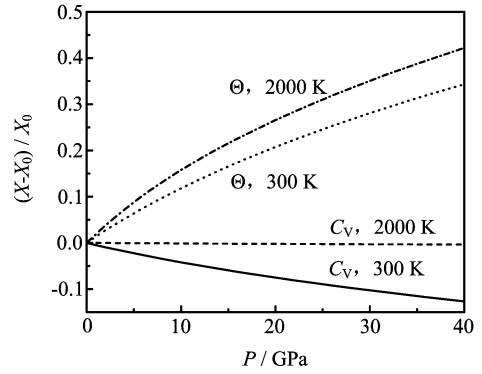

FIG. 5 Variation of thermodynamic parameters X with pressure and temperature, where X and X_0 are the Θ or C_V at any pressure and zero pressure at the temperature of 300 and 2000 K.

temperature and pressure are shown in Fig.7. It is obvious that γ shows weak dependence on temperature along the isobar. Upon compression, γ decreases significantly, but the temperature effects become less pronounced. In addition, the values of γ at high pressure remain nearly constant.

IV. CONCLUSION

The structural and thermodynamic properties of Zr_2AlC at high pressure and high temperature are studied via first principles DFT method. The equilibrium lattice parameters, bulk modulus and elastic constants at zero pressure are also obtained, which are consistent with the available theoretical data. The pressure dependences of the elastic constants, bulk modulus, shear modulus, Young's modulus, and Vickers hardness of Zr_2AlC are successfully obtained. From our analysis, it is found that Zr_2AlC is a brittle system with applied pressure. The Vickers hardness of Zr_2AlC decreases with increasing pressure. The direction dependence of Young's modulus shows that Zr_2AlC is an elastically anisotropic.

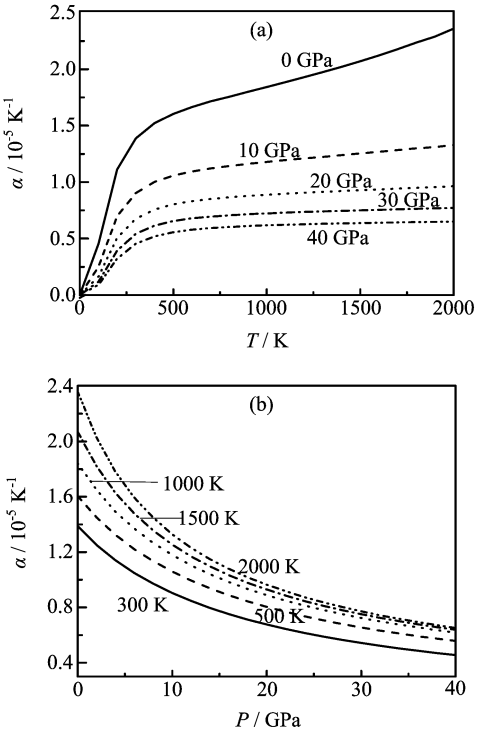

FIG. 6 Variation of the volume thermal expansion coefficient α with (a) temperature and (b) pressure for Zr_2AlC.

By using the quasiharmonic Debye model, the thermodynamic properties including the Debye temperature, heat capacity, volume thermal expansion coefficient, and Grüneisen parameter at high pressure and temperature are predicted for the first time. It is found that at a given temperature, the Debye temperature increases with increasing pressure. It is also shown that the volume thermal expansion coefficient and heat capacity converge to a nearly constant value at high pressure and temperature. For Grüneisen parameter, it is obvious that the temperature effects are weak along the isobar.

V. ACKNOWLEDGMENTS

This work was supportted by the National Natural Science Foundation of China (No.11447176 and

DOI:10.1063/1674-0068/28/cjcp1503032

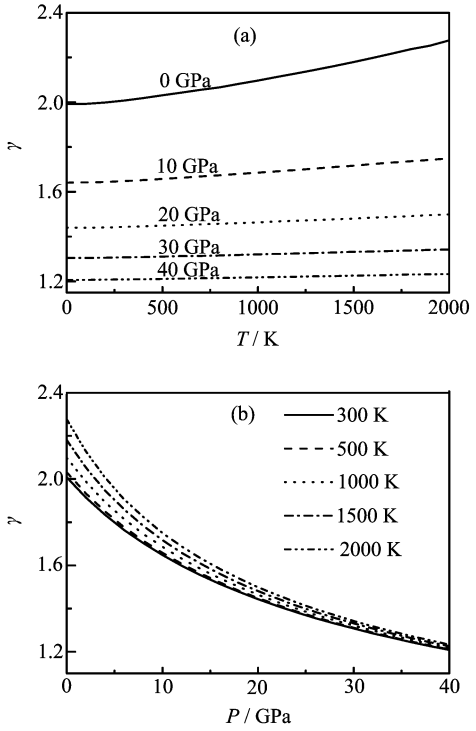

FIG. 7 Variation of the Grüneisen parameter γ with (a) temperature and (b) pressure for Zr_2AlC.

No.11447152), the National Natural Science Foundation of China and the China Academy of Engineering Physics (No.U1230201), and the Doctor Foundation of Southwest University of Science and Technology (No.13zx7137 and No.14zx7167).

[1] M. W. Barsoum, Prog. Solid State Chem. **28**, 201 (2000).
[2] J. Wang and Y. Zhou, Annu. Rev. Mater. Res. **39**, 415 (2009).
[3] P. Eklund, M. Beckers, U. Jansson, H. Högberg, and L. Hultman, Thin Solid Films **518**, 1851 (2010).
[4] N. I. Medvedeva, A. N. Enyashin, and A. L. Ivanovskii, J. Struct. Chem. **52**, 785 (2011).
[5] Z. M. Sun, Int. Mater. Rev. **56**, 143 (2011).
[6] J. M. Wang, J. Y. Wang, A. J. Li, J. J. Li, and Y. C. Zhou, J. Am. Ceram. Soc. **97**, 1202 (2014).
[7] H. Nowotny, Prog. Solid State Chem. **2**, 27 (1970).
[8] J. P. Palmquist, S. Li, P. O. A. Persson, J. Emmerlich, O. Wilhelmsson, H. Högberg, M. I. Katsnelson, B. Johansson, R. Ahuja, O. Eriksson, L. Hultman, and U. Jansson, Phys. Rev. B **70**, 165401 (2004).
[9] J. Etzkorn, M. Ade, and H. Hillebrecht, Inorg. Chem. **46**, 7646 (2007).
[10] C. Hu, F. Li, J. Zhang, J. Wang, J. Wang, and Y. Zhou, Scr. Mater. **57**, 893 (2007).
[11] R. S. Kumar, S. Rekhi, A. L. Cornelius, and M. W. Barsoum, Appl. Phys. Lett. **86**, 111904 (2005).
[12] D. Music, J. Emmerlich, and J. M. Schneider, J. Phys: Condens. Matter **19**, 136207 (2007).
[13] M. G. Brika, N. M. Avram, and C. N. Avram, Comput. Mater. Sci. **63**, 227 (2012).
[14] M. Romeo and R. Escamilla, Comput. Mater. Sci. **81**, 184 (2014).
[15] A. Yakoubi, L. Beldi, B. Bouhafs, M. Ferhat, and P. Ruterana, Solid State Commun. **139**, 485 (2006).
[16] A. Bouhemadou, R. Khenata, and M. Chegaar, Eur. Phys. J. B **56**, 209 (2007).
[17] M. D. Segall, P. J. D. Lindan, M. J. Probert, C. J. Pickard, P. J. Hasnip, S. J. Clark, and M. C. Payne, J. Phys.: Condens. Matter **14**, 2717 (2002).
[18] J. P. Perdew, K. Burke, and M. Ernzerhof, Phys. Rev. Lett. **77**, 3865 (1996).
[19] F. Birch, J. Geophys. Res. **83**, 1257 (1978).
[20] F. Luo, L. C. Cai, X. R. Chen, F. Q. Jing, and D. Alfè, J. Appl. Phys. **111**, 053503 (2012).
[21] Z. J. Wu, E. J. Zhao, H. P. Xiang, X. F. Hao, X. J. Liu, and J. Meng, Phys. Rev. B **76**, 054115 (2007).
[22] R. Hill, Proc. Phys. Soc. Lond A **65**, 350 (1952).
[23] X. Q. Chen, H. Y. Niu, D. Z. Li, and Y. Y. Li, Intermetallics **19**, 1275 (2011).
[24] S. F. Pugh, Philos. Mag. **45**, 823 (1954).
[25] J. R. Christman, *Fundamentals of Solid State Physics*, New York: Wiley, (1988).
[26] J. F. Nye, *Physical Properties of Crystals*, Oxford: Oxford University, (1985).
[27] M. A. Blanco, E. Francisco, and V. Luaña, Comput. Phys. Commun. **158**, 57 (2004).

DOI:10.1063/1674-0068/28/cjcp1503032